Temperature dependence of the dielectric function and the interband critical points of InSb

S. Logothetidis,* L. Viña, and M. Cardona
Max-Planck-Institut für Festkörperforschung, Heisenbergstrasse 1, D-7000 Stuttgart 80, Federal Republic of Germany
(Received 27 July 1984)

Measurements performed with a rotating-analyzer ellipsometer have been used to determine the dielectric function of undoped InSb between 1.2 and 5.6 eV in the temperature range 100 to 700 K. The critical energies of the critical points (CP's) E_1, $E_1+\Delta_1$, E_0', $E_0'+\Delta_0'$, E_2, $\Delta_5^{vu}-\Delta_5^{cu}$, $\Delta_5^{vl}-\Delta_5^{cu}$, E_1', and $E_1'+\Delta_1'$, and their dependence on temperature, have been obtained. Separate critical contributions in the E_0' region, which were assigned earlier to Γ- and Δ-symmetry transitions, have been resolved. The experimentally obtained CP energies have been fitted to the empirical expression given by Varshni and also to a phenomenological expression which follows from the Bose-Einstein statistical factor. The line-shape analysis of the derivative spectra allows us to obtain precise broadening parameters, amplitudes, and excitonic phase angles for the above-mentioned CP's. A decrease in these phase angles with increasing temperature is observed. It suggests a corresponding decrease of excitonic interaction effects with increasing temperature.

I. INTRODUCTION

InSb is an interesting semiconductor from the point of view of optical spectroscopy, band-structure theory, and optoelectronic applications. Because of the large atomic number of its constituents, relativistic effects [among others, spin-orbit (SO) splittings], are large for InSb and require elaborate relativistic band-structure calculations. Because of this, the critical-point structures in the visible and uv optical spectra show better-resolved SO splittings in InSb than in other zinc-blende-type semiconductors. Its small direct lowest gap ($\sim$0.2 eV) makes it an interesting material for optoelectronic applications as an ir detector and generator.

Interband transitions have been studied in InSb by means of reflectance[1–3] and transmission[4] spectroscopy, different reflectance-modulation schemes, such as piezoreflectance,[5] electroreflectance,[6] thermoreflectance,[7,8] magnetoreflectance,[9] and wavelength-modulated reflectance,[10–12] as well as by ellipsometry[13,14] and electron-energy-loss spectroscopy.[15] Recent angle-resolved photoemission work has given detailed experimental information on the k dependence of the valence bands.[16]

Several authors, using different optical techniques, have reported on the temperature dependence of interband transitions and, sometimes, of the corresponding optical constants of InSb. Transmission between 80 and 300 K,[4,5] reflectivity between 300 and 500 K,[1,2] and wavelength-modulated reflectance measurements[11] (80–300 K) have been performed near the fundamental gap[1,5] for the E_1 and $E_1+\Delta_1$,[1,4,5] and E_1, $E_1+\Delta_1$, and E_2 interband transitions.[11] However, considerable discrepancies exist among these data because the experimental results are rather sensitive to the resolution of the experimental techniques, the models used to interpret them, and the number of measured points.

Many band-structure calculations are available in the literature for diamond and zinc-blende semiconductors, but only a few apply to InSb.[17–20] One of them is presented in Fig. 1.[20] Some theoretical work on the temperature dependence of the band structure has been performed for InSb.[5,21] Two mechanisms are generally believed to be responsible for this temperature dependence, namely thermal expansion and the electron-phonon interaction.[21–23] These two mechanisms yield contributions of the same order, although the former is *usually* smaller than the latter. The effect of thermal expansion can be easily calculated from the usually known dependence of the band structure on volume and the expansion coefficient. Hence the primary theoretical interest has focused recently on the effect of the electron-phonon interaction. This effect can also be broken up into two contributions: the effect of the second-order electron-phonon interaction taken to first order (the so-called Debye-Waller terms), and the effect of the first-order electron-phonon interaction taken to second order (the Fan terms[24]). Early estimates showed that the Debye-Waller term accounts for most of the observed temperature dependence of the critical-point (CP) energies in the III-V compounds.[25–27] However, it has been recognized that both of these contri-

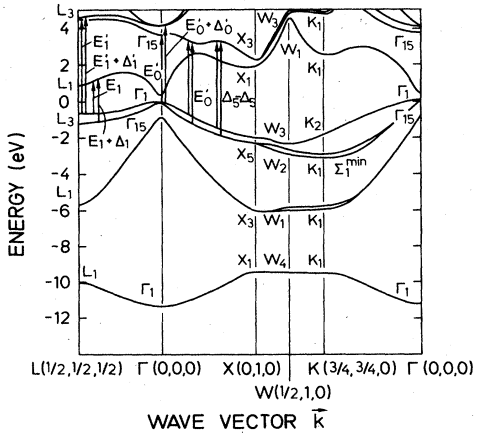

FIG. 1. Band structure of InSb in different directions of the Brillouin zone reproduced from Ref. 20. Arrows indicate interband transitions assigned to the observed structures.

butions[22,27] should be taken into account.

This paper presents the optical constants of undoped InSb determined with an automatic rotating-analyzer ellipsometer,[28] for several temperatures from 100 to 700 K in the photon-energy range 1.2—5.6 eV. We investigate, in this manner, the higher interband transitions E_1, $E_1+\Delta_1$, E_0', $E_0'+\Delta_0'$, E_2, Δ_5^{vu}-Δ_5^{cu}, and Δ_5^{vl}-Δ_5^{cu}, and E_1' and $E_1'+\Delta_1'$. A line-shape analysis of the numerically obtained second-derivative spectra of the complex dielectric function ($\epsilon=\epsilon_1+i\epsilon_2$) near the CP allows us to obtain precisely the critical energies (E), the broadening parameters (Γ), the amplitudes (A), and the phases (ϕ) of the CP's as a function of temperature. A shift of the CP's to lower energies and an increase in their broadening parameters Γ, as well as a decrease of the excitonic interaction with increasing temperature, have been observed. In Sec. II the experimental details are described, and in Sec. III the results of our measurements are presented and discussed.

II. EXPERIMENTAL DETAILS

The measurements were performed on a thin undoped crystal of InSb (1×10^{14} e/cm^3, mobility 5.3×10^5 $cm^2V^{-1}sec^{-1}$ at 77 K, and ~0.1 Ω cm resistivity) with a (110)-surface orientation, in the temperature range 100—700 K. The mechanical polishing of the surfaces followed the procedure described in Ref. 29. The etching procedure was chosen after several tries so as to optimize ϵ_2 at the E_2 critical point (at ~4 eV).[30] We settled for a rinse in methanol followed by etch with a 5-vol% solution of HF in methanol and finally an etch with a 50-vol% solution of HCl in methanol. The treatment was repeated until the largest value of ϵ_2 at E_2 ($\epsilon_2\simeq21$) was obtained. During the etching procedure the samples were kept at room temperature in a windowless cell in flowing dry N_2 so as to minimize surface contamination. We also investigated a (100) surface with the same etchants used for the (110) surface: The values of $\epsilon_2(\omega)$ at E_2 were, for the (110) surface, at least one unit larger than those for (100) orientation. Hence we used the (110) samples in our measurements. An etching procedure with exposure to an HCl-methanol (1:1) solution for a long time[13,31] did not give us the best values of $\epsilon_2(\omega)$ at E_2. After etching, the sample was placed as quickly as possible in the cryostat so as to minimize oxide formation.

Owing to the formation of natural oxides on the InSb surfaces and the preferential etching characteristics,[14,32–34] a careful etching procedure is necessary to produce the sharpest substrate-ambient discontinuities in order to facilitate the use of the two-phase model[35] for the evaluation of the optical constants from the ellipsometric measurements. On its way from the ellipsometer table to the cryostat, the sample was kept in flowing dry N_2, and at the last moment was again rinsed with methanol.

The sample was glued to the cold finger of the cryostat with "Leitsilber" cement.[36] We closed the cryostat in a N_2 atmosphere and then pumped it with a diffusion pump and an ion pump until the pressure was 10^{-6} Torr. The entire cryostat was then baked out to ~200 °C. In this way we attained a vacuum better than 2×10^{-8} Torr for all temperatures at which measurements were performed.

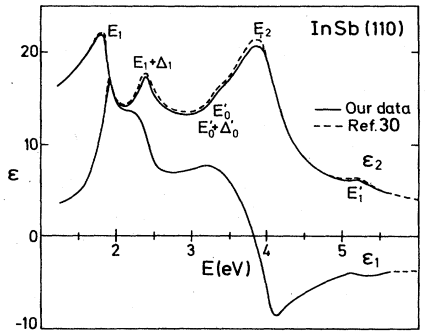

FIG. 2. Solid lines: real (ϵ_1) and imaginary (ϵ_2) parts of the dielectric function measured for a (110) surface of InSb at room temperature. Dashed lines: corresponding results reported in Ref. 30.

This was necessary in order to avoid reflectivity changes due to condensation of vapors on the sample at low temperature.[29,37]

The details concerning the ellipsometer, including mirror optics, light sources, photomultipliers, and the cryostat, as well as the alignment, precision, and stability of the apparatus, have been presented in Ref. 29.

III. RESULTS AND DISCUSSION

Figure 2 shows the spectrum of the dielectric function at room temperature obtained by us for the (110) surface of undoped InSb (solid line) after etching with methanol, HF-methanol (1:20), and HCl-methanol (1:1) solutions. The agreement with measurements in Ref. 30 for InSb of the same orientation (dashed lines) is quite good. Small discrepancies are probably due to differences in surface conditions after the chemical treatment. The real and imaginary parts of the complex dielectric function are shown for selected temperatures in Figs. 3 and 4, respectively. These dielectric functions were calculated from the complex reflectance ratio with a three-phase model. We assumed that a thin oxide layer was still present and es-

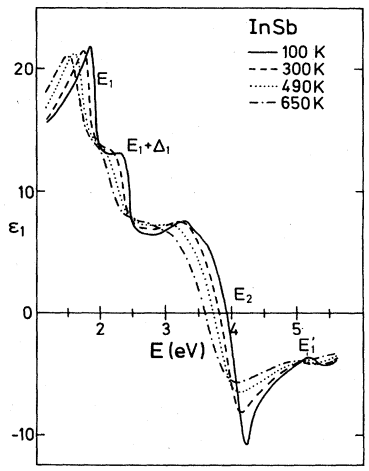

FIG. 3. Real part of the dielectric function of InSb at: 100 (——), 300 (— — —), 490 (· · ·), and 650 K (—·—·—).

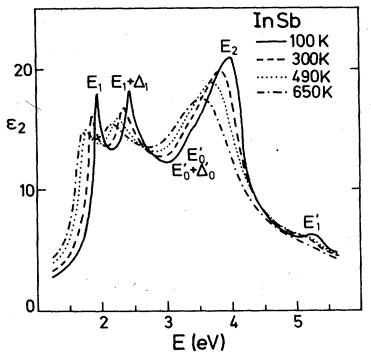

FIG. 4. Imaginary part of the dielectric function of InSb. The symbols are the same as in Fig. 3.

timated[29] its thickness to be 6±2 Å. We supposed that this undesired oxide was InSb native oxide and we used, to correct its effects, dielectric function data from Ref. 13. The main characteristics of the data in Figs. 3 and 4 are the shift to low energy and the broadening of the major CP's E_1, $E_1+\Delta_1$, E_0', E_2, and E_1'. The E_1, $E_1+\Delta_1$, and E_2 structures are clearly observed at all temperatures from 100 and 650 K. Other weaker structures, such as E_0' and $E_0'+\Delta_0'$, as well as Δ_5^{vl}-Δ_5^{cu}, E_1', and $E_1'+\Delta_1'$ (see Sec. III D and Fig. 5), are difficult to distinguish in these figures.

We have used second derivatives of the complex dielectric function, numerically computed from the ellipsometric data, to study the change of the CP's with temperature. The existence of an important contribution of excitonic effects, which was recognized earlier by several authors,[10,12] is taken into account by assuming a mixture of two different CP's, M_j and M_{j+1}.[38,39] Figure 5 shows the second-derivative spectrum computed from our experimentally obtained imaginary part of the complex dielectric function at 100 K, together with best fits using the standard critical-point line shapes. The model assumed for the fitting of derivative spectra around two-dimensional (2D) and three-dimensional (3D) critical points[39–41] is

$$\epsilon \sim C - \ln(E-\omega-i\Gamma)e^{i\phi} \quad \text{for a 2D critical point} \tag{1a}$$

(minimum or saddle point), and

$$\epsilon \sim C + i(\omega-E+i\Gamma)^{1/2}e^{i\phi} \quad \text{for a 3D critical point} \tag{1b}$$

(M_0 or M_1), where E denotes the CP energy and Γ is the broadening parameter. In the absence of excitonic effects, the phase angle ϕ should be zero for an M_0 or minimum critical point, and $\pi/2$ for an M_1 or saddle point. We have used Eqs. (1a) and (1b) to fit the CP's at different temperatures.

Figure 5 reveals considerable structure which is difficult to see in Figs. 3 and 4. In the region from 3 to 4 eV two sets of two peaks are seen. The first and the third are labeled E_0' and $E_0'+\Delta_0'$ in the literature. For reasons which will become apparent below, we label the second and the fourth ones $E_0'(\Delta)$ and $E_0'+\Delta_0'(\Delta)$.

The critical-point energies obtained from our fit to the E_1, $E_1+\Delta_1$, $E_0'(\Delta)$, $E_0'+\Delta_0'(\Delta)$, E_2, and E_1' CP's as a function of temperature are shown in Figs. 6 and 7. These temperature dependences were analyzed with two different models: Varshni's empirical relation,[42] and a phenomenological expression based on the Bose-Einstein statistical factor which should take into account electron-phonon interactions with phonons of average frequency Θ:[29]

$$E(T)=E(0)-\alpha T^2/(T+\beta) \quad \text{(Varshni)}, \tag{2a}$$

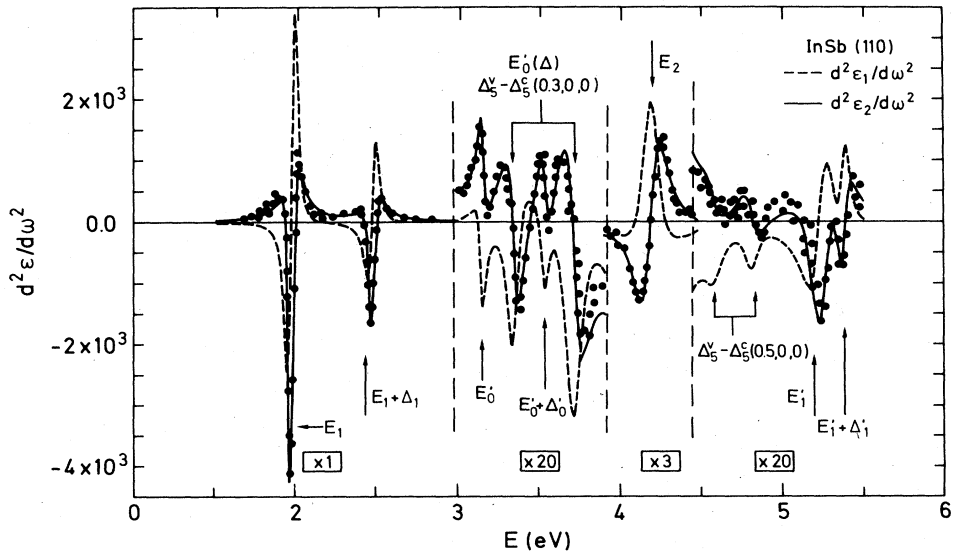

FIG. 5. Fits to the second derivatives of the real (dashed line) and imaginary (solid line) parts of the dielectric function of InSb as a function of photon energy at 100 K. The dots represent data for $d^2\epsilon_2/d\omega^2$. The vertical scale for the region of the E_0' and E_1' transitions has been expanded by a factor of 20, and that for the E_2 transitions, by a factor of 3.

TABLE I. Values of $E(0)$, α, and β parameters obtained by fitting the critical-point energies vs temperature with Eq. (2a). Values of E_B, α_B, and Θ parameters obtained by fitting with Eq. (2b), and, finally, values for the E_2 CP parameters obtained from a linear fit: $E(T)=E_L-\gamma T$.

	$E(0)$ (eV)	α ($\times 10^{-4}$ eV K^{-1})	β (K)	E_B (eV)	α_B (meV)	Θ (K)	E_L (eV)	γ ($\times 10^{-4}$ eV K^{-1})
E_1	2.00(1)	6.84(50)	132(80)	2.075(50)	91(30)	272(90)		
$E_1+\Delta_1$	2.49(1)	6.46(50)	170(70)	2.56(4)	88(27)	286(75)		
$E_0'(\Delta)$	3.37(4)	5.0(10)	115(90)	3.43(2)	68(5)	272		
$E_0'+\Delta_0'(\Delta)$	3.74(5)	4.8(10)	104(90)	3.79(2)	71(10)	286		
E_2							4.240(4)[a]	5.4(5)[a]
							4.272(7)[b]	7.5(4)[b]
E_1'	5.245(30)	8.31(30)	250(150)	5.383(85)	163(120)	413(185)		

[a]With a 2D maximum.
[b]2D maximum mixed with a 2D saddle point.

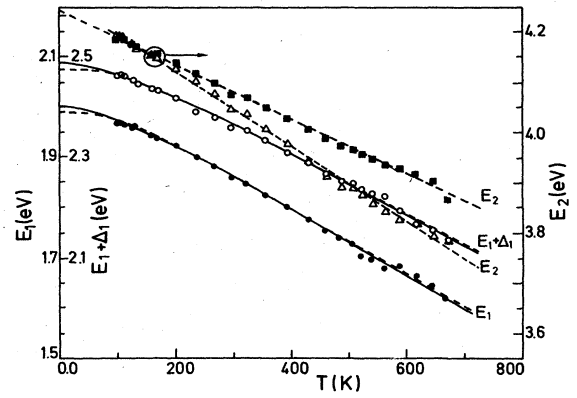

FIG. 6. Temperature dependence of the critical-point energies of InSb: the solid circles correspond to the E_1 critical point (outer scale on the left), and open circles, to the $E_1+\Delta_1$ critical point (inner scale on the left). The squares and triangles (scale on the right) show the results of two different fits to the E_2 structure as described in Sec. III C: The squares correspond to fits to a 2D maximum and the triangles to fits with a mixture of a 2D saddle point and maximum. The solid lines represent the best fits with Eq. (2a); the dashed lines for the E_1 and $E_1+\Delta_1$ critical points correspond to the fit with Eq. (2b) and, for the E_2 critical point, to a linear fit. Typical error bars for the experimental points are given in Table III.

$$E(T)=E_B-\alpha_B\left[1+\frac{2}{e^{\Theta/T}-1}\right]\quad\text{(Bose-Einstein)}\,,\qquad(2b)$$

A least-squares-fitting procedure was used to determine the parameters of these two equations. Values of these constants are listed in Table I with the corresponding uncertainties representing 95% reliability. A lineary dependence of the CP energy on temperature is found at high temperatures. This dependence usually flattens out at low temperatures, a fact which is well represented by either Eq. (2a) or (2b).

We have used an expression analogous to Eq. (2b) in or-

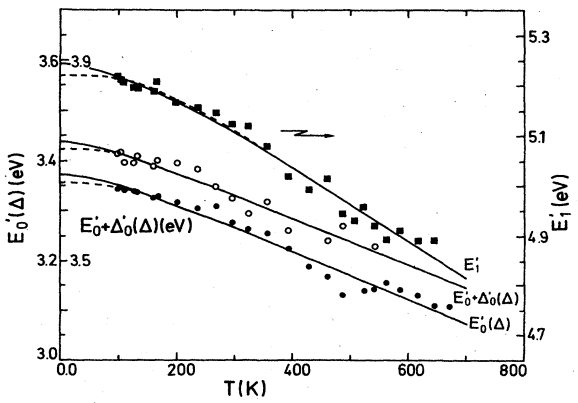

FIG. 7. Temperature dependence of the $E_0'(\Delta)$ (solid circles), $E_0'+\Delta_0'(\Delta)$ (open circles), and E_1' (squares) critical-point energies of InSb. The solid lines represent the best fits with Eq. (2a), while the dashed lines correspond to a fit with Eq. (2b). Typical error bars for experimental points are given in Table III.

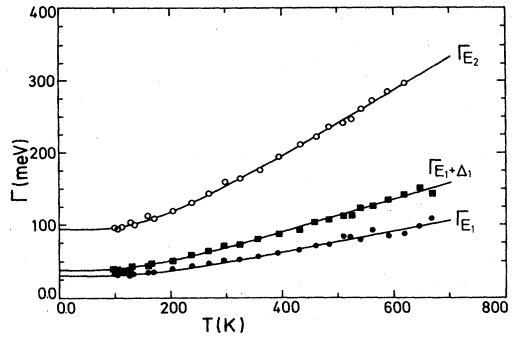

FIG. 8. Temperature dependence of the broadening parameters of the critical points. The solid circles correspond to the E_1 transition, the squares to the $E_1+\Delta_1$ transitions, and the open circles to the E_2 transitions. The solid lines represent the best fits with Eq. (3) with the parameter Θ fixed as described in the text. Typical error bars for experimental points are given in Table IV.

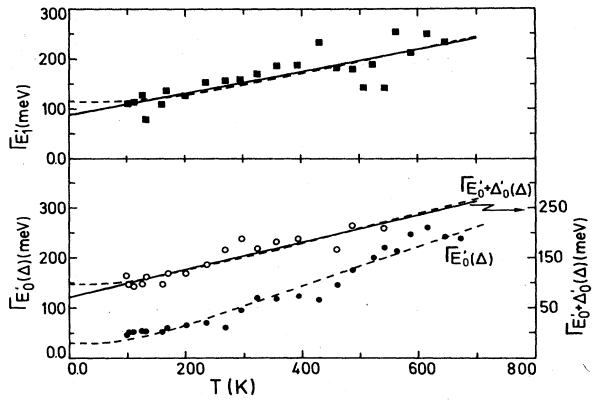

FIG. 9. Temperature dependence of the broadening parameters of the $E_0'(\Delta)$, $E_0'+\Delta_0'(\Delta)$, and E_1' critical points. The solid and open circles correspond to the $E_0'(\Delta)$ and $E_0'+\Delta_0'(\Delta)$ transitions, respectively, while the squares correspond to the E_1' transitions. The dashed lines represent the best fits with Eq. (3) (where the parameter Θ is fixed). The solid lines represent the corresponding linear fits for $E_0'+\Delta_0'(\Delta)$ and E_1'. Typical error bars for experimental points are given in Table IV.

der to fit the temperature dependence of the Lorentzian broadening parameter Γ for the different CP's (Ref. 29) shown in Figs. 8 and 9,

$$\Gamma(T)=\Gamma_1+\Gamma_0\left[1+\frac{2}{e^{\Theta/T}-1}\right]. \tag{3}$$

The values of Γ obtained for E_1, $E_1+\Delta_1$, and E_2 (Fig. 8 and Table II) are sufficiently accurate to allow a meaningful fit of Γ_0, Γ_1, and Θ in Eq. (3). The data for E_0', $E_0'+\Delta_0'$, and E_1' (Fig. 9), however, show so much scatter that a meaningful determinatoin of the three fitting parameters is not possible. Hence, for the fit, we have chosen to fix the average phonon temperature Θ at the value found from the shifts of these critical points versus temperature.

A. E_1 and $E_1+\Delta_1$ transitions

The E_1 and $E_1+\Delta_1$ transitions should take place along Λ or at L, as in other similar materials.[20,43–46] As can be seen in Table III, our results for the energy of those CP's at 100 K obtained from a fit with Eq. (1b) compare well with wavelength-modulated-reflectance results obtained at 80 K,[12] and also with electroreflectance[6] and ellipsometric results[13] if temperature differences are corrected for.

Since the transverse reduced mass $m_\perp$ of the critical points responsible for the E_1 and $E_1+\Delta_1$ transitions is much smaller than its longitudinal counterpart $m_\parallel$ (Refs. 6 and 39) (for InSb, $m_\parallel\simeq 1$ and $m_\perp\simeq 0.04$), these critical points can be treated as two dimensional. Strictly speaking, there are two possibilities: either a 3D M_1 critical point at L, or a combination of an M_0 critical point at L and an M_1 critical point at a general Λ, very close in energy. Band-structure calculations are not sufficiently reliable to discriminate between these possibilities.[20] The difference, however, becomes merely academic if one treats the problem as a 2D minimum: this difference may actually be lost within the Lorentzian broadening of the critical points.[29] Recently, the two- or three-dimensional character of these critical points has been investigated ellipsometrically versus temperature for Ge (Ref. 29) and α-Sn (Ref. 40). At all temperatures, the best fit was found with a 2D CP. The same situation holds for our fits of the E_1 and $E_1+\Delta_1$ transitions of InSb with either a 2D or 3D model. We always obtain a better fit with the 2D model. In view of this, we have used a 2D line shape to describe the E_1 and $E_1+\Delta_1$ structures. We have been able to simultaneously fit the E_1 and $E_1+\Delta_1$ CP's at all temperatures with a mixture of a 2D minimum and a saddle point [Eq. (1a) with $0<\phi<\pi/2$]. Eight different adjustable parameters, four for each structure (A, E, Γ, and

TABLE II. Values of the parameters obtained by fitting the broadening parameters with Eq. (3), and $\Gamma=\Gamma_L+\gamma T$. The parameter Θ has been fixed to have the same values as in Table I.

	Γ_1 (meV)	Γ_0 (meV)	Θ (K)	Γ_L (meV)	γ ($\times 10^{-4}$ eV K^{-1})
$\Gamma(E_1)$	9(3)	18(1)	272	15(3)	1.24(9)
$\Gamma(E_1+\Delta_1)$	2(2)	31(1)	286	14(3)	1.99(9)
$\Gamma(E_0'(\Delta))$	−29(18)	61(6)	272	3(3)	3.56(40)
$\Gamma(E_0'+\Delta_0'(\Delta))$	60(20)	39(10)	286	74(12)	2.7(6)
$\Gamma(E_2)$	−16(14)	112(16)	463(50)	48(5)	3.88(1)
$\Gamma(E_1')$	65(30)	52(16)	413	88(10)	2.3(5)

TABLE III. Critical-point energies in InSb measured at several temperatures. All the energies are in eV. (RT denotes room temperature.)

T (K)	E_1	$E_1+\Delta_1$	E_0'	Δ_5^{vu}-Δ_5^{cu} (0.3, 0, 0)	$E_0'+\Delta_0'$	Δ_5^{vl}-Δ_5^{cu} (0.3, 0, 0)	E_2	Δ_5^{vu}-Δ_5^{cu} (0.5, 0, 0)	Δ_5^{vl}-Δ_5^{cu} (0.5, 0, 0)	E_1'	$E_1'+\Delta_1'$
RT	1.880[a]	2.380[a]	3.16[a]	3.49[a]			4.08[a]	4.66[a]		5.25[a]	
RT	1.800[b]	2.400[b]		3.40[b]			4.10[b]				
RT	1.890[c]	2.440[c]									
RT	1.820[d]	2.380[d]					4.13[d]				
RT	1.835[e]	2.350[e]									
RT	1.872(2)[f]	2.374(10)[f]									
100							4.12[g]	4.60[g]	4.84[g]	5.39[g]	
80	1.972[h]	2.470[h]	3.18[h]	3.36[h]	3.56[h]	3.74[h]	4.04[h]	4.64[h]	4.84[h]		
80	1.980[i]	2.500[i]	3.33[i]		3.70[i]		4.16[i]	4.70[i]			
77	1.900[j]	2.400[j]									
5	1.983[k]	2.478[k]	3.39[k]		3.78[k]		4.23[k]	4.75[k]	4.92[k]	5.336[k]	
100	1.968(1)[l]	2.466(4)[l]	3.14(1)[m]	3.348(9)[m]	3.533(6)[m]	3.72(2)[m]	4.186(2)[n]	4.56(3)[n]	4.81(4)[l]	5.22(3)[l]	5.38(2)[l]

[a]Reference 6.
[b]Reference 43.
[c]Reference 4.
[d]J. Tauc and A. Abraham, in *Proceedings of the International Conference on the Physics of Semiconductors* (Czechoslovakia Academy of Sciences, Prague, 1960), p. 375.
[e]Reference 2.
[f]Reference 13.
[g]Reference 8.
[h]Reference 12.
[i]Reference 44.
[j]Reference 10.
[k]Reference 11.
[l]Present work with a mixture of 2D CP's.
[m]Present work with a mixture of 3D CP's.
[n]Present work with a 2D maximum CP.

TABLE IV. Experimental and theoretical spin-orbit splittings for InSb, all in meV.

T (K)	Δ_0	Δ_1	$\Delta_0'(\Gamma)$	$\Delta_5^{vu}-\Delta_5^{vl}$ (0.3, 0, 0)	$\Delta_5^{vu}-\Delta_5^{vl}$ (0.5, 0, 0)	Δ_1'	$\Delta_1+\Delta_1'$
				Experimental			
RT		560[a]					
RT	820[b]	500[b]		330[b]			
RT		600[c]					
RT	803[d]	500[d]					
RT		502(12)[e]					
80		510[f]					
80		498[g]	380[g]	380[g]			
80		500[h]					
80		502[i]		370[i]			
5	820[j]	495[j]		390[j]		170[j]	630[j]
4.2	980[k]						
100	850[l]	498(4)[l]	392(12)[l]	396(16)[l]	250(40)[l]	154(28)[l]	
				Theoretical			
		480[a]					
	820[b]	530[b]		450[b]		330[b]	
	770[m]	490[m]	470[m]			240[m]	
	820[n]	480[n]	430[n]	400[n]	290[n]	230[n]	710[n]

[a]J. Tauc and A. Abraham, in *Proceedings of the International Conference on the Physics of Semiconductors* (Czechoslovakia Academy of Sciences, Prague, 1960), p. 375.
[b]Reference 6.
[c]Reference 43.
[d]S. O. Sari, Solid State Commun. **12**, 705 (1973).
[e]Reference 13.
[f]Reference 7.
[g]Reference 12.
[h]Reference 10.
[i]Reference 44.
[j]Reference 11.
[k]S. Zwerdling, W. H. Kleiner, and J. P. Theriault, J. Appl. Phys. **32**, 2118 (1961).
[l]Present work.
[m]Reference 60, calculated with the relativistic orthogonalized-plane-wave method.
[n]Reference 20.

ϕ), have been obtained for each temperature. The SO splitting Δ_1 is 498(4) meV (Table IV), in excellent agreement with Ref. 12. A variation of Δ_1 smaller than 10 meV in the temperature range 100—700 K, of the same order as the experimental error, emphasizes the temperature independence of this parameter which follows from its intra-atomic origin.

Figure 6 shows the temperature dependence of the E_1 and $E_1+\Delta_1$ CP energies; these curves are nearly parallel to each other, as can be seen by the small differences in the slopes of the linear portions (Table I). In Fig. 6 the solid lines represent the best fit to Eq. (2a). The values of the β parameter are close to the Debye temperature of InSb [150 K at room temperature (RT) according to Ref. 47]. The small value of this parameter, together with the large error in estimating it, results in nearly linear behavior for these two structures in the entire temperature range. This is a general property of the temperature dependence of all the CP energies in InSb. The dashed lines in Fig. 6 for E_1 and $E_1+\Delta_1$ correspond to the best fit to Eq. (2b). The parameter Θ in this model should correspond to an average phonon frequency (see Table I).[29,48] It is somewhat larger than the average frequency obtained from dispersion relations.[49] This large value of Θ indicates that the major contribution to the gap shifts at high temperatures comes from optical phonons.

Several authors have observed that the spectra of InSb in the neighborhood of the E_1 and $E_1+\Delta_1$ structures cannot be simply explained in the framework of the one-electron approximation with lifetime-broadening corrections, and have suggested that the Coulomb interaction should play a strong role.[10,12,50] These effects can be described in a simple way with the help of the phase factor of Eq. 1(b).[39,41] We have included this phase factor and used ϕ as the fourth adjustable parameter in our fits. We show in Fig. 10 the temperature dependence of the phase angle ϕ for the E_1 (open circle) and $E_1+\Delta_1$ (triangle) CP's. This dependence is basically the same for both critical points at low T, although at high T it decreases somewhat faster for E_1 than for $E_1+\Delta_1$. We note that, at low T, ϕ reaches values as high as 105°, which, if taken literally, would correspond to a mixture of *saddle point* and maximum critical point. We note that such large values of ϕ are also found at low temperatures for other

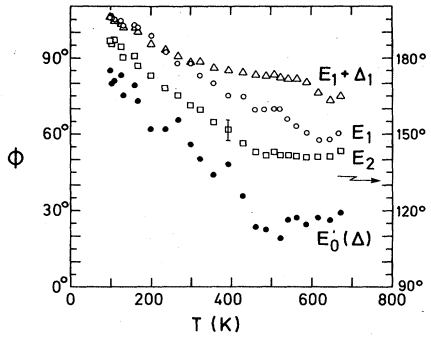

FIG. 10. Temperature dependence of the phase angle ϕ defined in Eqs. (1) for the E_1 (open circles), $E_1+\Delta_1$ (triangles), E_2 (squares), and $E_0'(\Delta)$ (solid circles) critical points. The rhs scale corresponds to the E_2 points.

semiconductors of the family.[40,51,52] Unfortunately, no quantitative theory for the decrease in ϕ with increasing temperature is available.

The amplitude A depends on interband momentum matrix elements and effective masses. Within the one-electron approximation (i.e., if $\phi=0$), it is approximately given by[53]

$$A_{E_1}\simeq\frac{44(E_1+\Delta_1/3)}{a_0E_1^2}=3.75\ ,$$
$$A_{E_1+\Delta_1}\simeq\frac{44(E_1+2\Delta_1/3)}{a_0(E_1+\Delta_1)^2}=2.57\ , \tag{4}$$

where a_0, the lattice constant, is in Å, and E is in eV. The values $A_{E_1}=4.5(3)$ and $A_{E_1+\Delta_1}=2.5(3)$ (dimensionless units of dielectric function) are found from our fitting at 100 K. A ratio $(A_{E_1}/A_{E_1+\Delta_1})_{\text{expt}}=1.77$ is found from the experimental values, as compared to the ratio obtained from Eqs. (4), $(A_{E_1}/A_{E_1+\Delta_1})_{\text{calc}}=1.46$. Calculations for Si (Refs. 54 and 55) and GaAs (Ref. 56) show that the k-linear term for k perpendicular to $\langle 111\rangle$ can significantly increase the strength of the E_1 and E_1' structures relative to $E_1+\Delta_1$ and $E_1'+\Delta_1'$. This effect should be small ($\sim 10\%$) for materials with large Δ_1 such as InSb.[56] On the other hand, Hanke and Sham[57] have shown that excitonic effects can also increase the strength of the E_1 structure.

From the measured values of A_{E_1} and $A_{E_1+\Delta_1}$ vs T, we obtain

$$\frac{A_{E_1}}{A_{E_1+\Delta_1}}=(1.88\pm0.08)-(4.04\pm2)\times10^{-4}T \tag{5}$$

for temperatures between 100 and 550 K. If we extrapolate Eq. (5) to $T=650$ K, where excitonic effects should be very weak (see Fig. 10), we find $(A_{E_1}/A_{E_1+\Delta_1})_{\text{expt}(T=650\text{ K})}\simeq1.62\pm0.08$. The calculated value of this ratio, including a correction for terms linear in k with a matrix element Π of $\vec{p}$ equal to that for Si ($\Pi\sim0.1$ bohr^{-1}), becomes $1.46\times1.13\simeq1.65$, in rather good agreement with the experimental value (Π represents the matrix element of the average component of $\vec{p}$ perpendicular to [111] between the two components of the Λ_3 valence wave functions).[54]

Figure 8 shows the temperature dependence of the broadening parameters fitted with Eq. (3). As already mentioned, we have fixed the parameter Θ to have the same value as obtained for the CP energies (see Tables I and II). In Table II we also give the average slope $(d\Gamma/dT)$ for the different CP's.

B. E_0' transitions

Detailed analysis of low-temperature modulated-reflectance data of InSb (Refs. 11 and 12) and similar materials[45,46,58] in the E_0' region shows the existence of two doublets. Comparison with band-structure calculations[6,20] suggests that the splitting of each of these doublets originates from critical points at Γ ($\Gamma_8^v\rightarrow\Gamma_7^c$, Γ_8^c) and also at points in the Δ direction (Δ_5^{vl}, $\Delta_5^{vu}\rightarrow\Delta_5^{cu}$). Within this interpretation the separation between the two doublets Δ_0' would have different origins for the first and second components of the doublets. For the $E_0'(\Gamma)$-$E_0'+\Delta_0'(\Gamma)$ pair it would correspond to the spin-orbit splitting of the Γ_{15} conduction bands, while for the $E_0'(\Delta)$-$E_0'+\Delta_0'(\Delta)$ pair it would correspond to the splitting of the top valence bands at the Δ point at which the transitions occur [around 30% of the Γ-X separation away from Γ (Ref. 20)]. By examining the band structure of Fig. 1, one concludes that these splittings are nearly equal (~0.4 eV) for InSb, although $\Delta_0'(\Gamma)$ should be slightly larger than $\Delta_0'(\Delta)$. These doublets are also observed in our low-temperature data (Fig. 5) in the (3—4)-eV region. If we assign the first and third structures to $E_0'(\Gamma)$ and $E_0'+\Delta_0'(\Gamma)$, we obtain an SO splitting $\Delta_0'(\Gamma)=392(12)$ meV. The other two singularities can be attributed to $E_0'(\Delta)$ and $E_0'+\Delta_0'(\Delta)$ transitions at $(2\pi/a)(0.3,0.0,0.0)$: an SO splitting $\Delta_0'(\Delta)=369(16)$ meV is found. These splittings are in reasonable agreement with those calculated in Ref. 20: $\Delta_0'(\Gamma)=430$ meV and $\Delta_0'(\Delta)=400$ meV.

We have also identified the structure between 4.5 and 5 eV in Fig. 5 as transitions along the Δ direction of the Brillouin zone. In Ref. 20, a doublet at $(2\pi/a)(0.5, 0.0, 0.0)$ with an SO splitting of 290 meV has been obtained in this region, again in good agreement with our result of 250(40) meV. Our experimental splittings for the three doublets just discussed are about 40 meV smaller than those calculated.

In earlier works,[6,11,12] the last doublet of Fig. 5 (4.56—4.81 eV) has not been resolved in its two counterparts, and has been assigned to the $E_2+\delta$ structure[6] (Δ_5^{vl}-Δ_5^{cu} close to the X point). Only in the thermoreflectance study of Ref. 8, where the assignment as here was also made, fine structure was observed at 4.6—4.84 eV, in rather good agreement with the present results. A very weak structure in the high-energy wing of the E_2 CP is also seen in Fig. 5. Its energy location could correspond to the $E_0'+\Delta_0'+\Delta_0$ CP, giving $\Delta_0\simeq850$ meV, in agreement with other experimental and theoretical determinations (see Table IV).

The E_0' structures were analyzed with a mixture of M_0 and M_1 3D critical points. The linewidths obtained at 100 K are listed in Table V. The temperature dependence

TABLE V. Broadening parameters of interband transitions in InSb. All values are in meV at 100 K.

$\Gamma(E_1)$	34(1)
$\Gamma(E_1+\Delta_1)$	40(1)
$\Gamma(E_0')$	32(12)
$\Gamma(\Delta_5^{vu}\text{-}\Delta_5^{cu}(0.3,0,0))$	53(9)
$\Gamma(E_0'+\Delta_0')$	39(10)
$\Gamma(\Delta_5^{vl}\text{-}\Delta_5^{cu}(0.3,0,0))$	98(16)
$\Gamma(E_2)$	96(4)
$\Gamma(\Delta_5^{vu}\text{-}\Delta_5^{cu}(0.5,0,0))$	90(40)
$\Gamma(\Delta_5^{vl}\text{-}\Delta_5^{cu}(0.5,0,0))$	80(25)
$\Gamma(E_1')$	98(27)
$\Gamma(E_1'+\Delta_1')$	53(28)

found for the average phase angle ϕ is shown, in Fig. 10, to follow the general trend for this parameter. The critical point is nearly M_1 at low temperatures and nearly M_0 at high temperatures. The temperature dependence of the $E_0'(\Delta)$ and $E_0'+\Delta_0'(\Delta)$ energies is plotted in Fig. 7 and fitted with both Eqs. (2a) (solid lines) and (2b) (dashed lines). Measurements at liquid-He temperature would help to decide which fit is better. The parameter Θ obtained from the fit with Eq. (2b) is, with rather large error bars, the same as that found for the E_1 and $E_1+\Delta_1$ structures (see Table I). The same applies to the parameters β of the fit with Eq. (2a). The temperature dependence of the broadening parameters Γ of the $E_0'(\Delta)$ and $E_0'+\Delta_0'(\Delta)$ structures is shown in Fig. 9. Within the experimental error, $\Gamma_{E_0'+\Delta_0'(\Delta)}$ can be fitted by a straight line, while some curvature is seen for $\Gamma_{E_0'(\Delta)}$ at low temperatures. The dashed line for $\Gamma_{E_0'(\Delta)}$ corresponds to the fit with $\Theta=272$ K, the value used for the fit of the temperature dependence of the energy of this CP.

C. E_2 transitions

The more pronounced structure in the region 3.0—4.5 eV is labeled E_2 (see Fig. 4). This peak, dominant in the $\epsilon_2(\omega)$ spectra of similar materials, corresponds to an extended region of k space around the point $(2\pi/a)(0.7, 0.2, 0.2)$.[20] Different models can be used to fit the structure corresponding to the E_2 CP, yielding fits of similar quality. Not only CP's of different dimensionality, as pointed out in Ref. 29, but also different 2D models describe this structure. We are able to fit this CP with 1D, 2D, or 3D models, allowing for a phase angle ϕ, and obtained the same dependence of the CP energy with T (-7.5×10^{-4} eV K^{-1}). However, a pure 2D maximum, which also gives a good fit and the same dependence of broadening on temperature, yields a quite different T dependence of the E_2 CP (-5.43×10^{-4} eV K^{-1}), as can be seen in Fig. 6 and Table VI. Owing to this fact and to the complicated character of this structure, care must be taken in analyzing its line shape. The best representation was obtained with a mixture of a 2D saddle point and maximum, a fact that is confirmed by similar results in Ge (Ref. 29) and α-Sn (Ref. 40).

The temperature dependence for the E_2 CP obtained from this fit is displayed in Fig. 6, together with that of the E_1 and $E_1+\Delta_1$ CP's. This dependence is practically linear, in the absence of data at lower temperatures, and thus the fitting with Eqs. (2a) and (2b) fails to give meaningful values of the Θ and β parameters. We have plotted Γ_{E_2} vs T in Fig. 8 and fitted it with Eq. (3). (In this case we were able to use Θ as a free parameter.) The Debye temperature as well as the mean frequency of phonons taking part in the scattering process decrease in the series diamond—Ge—Si—α-Sn—InSb.[59] If the parameters β and Θ from our fits are related to these quantities, they should decrease by the same amount. This is borne out by the experiments: a ratio of 1.9 is found between the Debye temperatures of Ge and InSb,[59] and the corresponding average ratio between our β-fit parameters is about 2.1.[29] The same can be said of the mean phonon frequencies and the Θ parameters. As the quadratic contribution in Eqs. (2) is important for β and Θ large compared with T [Eqs. (2a) and (2b)], this contribution shifts to low temperature as β

TABLE VI. Linear temperature coefficients of critical-point energies in InSb; all values in 10^{-4} eV/K.

$-dE_1/dT$	$-d(E_1+\Delta_1)/dT$	$-dE_0'(\Delta)/dT$	$-d(E_0'+\Delta_0')(\Delta)/dT$	$-dE_2/dT$	$-dE_1'/dT$
		Experimental			
4.4(4)[a]				3.6(4)[a]	
5.3(3)[b]	4.9(3)[b]			5.4[b]	
4.0(2)[c]	3.6(2)[c]				
6.2(1)[d]	5.65(10)[d]	4.6(4)[d]	4.4(6)[e]	5.4(6)[f]	5.6(5)[d]
				7.5(4)[f]	
		Theoretical			
				6.9[g]	
3.4[h]				3.0[h]	

[a]Reference 11, between 80 and 300 K.
[b]Reference 2, between 300 and 500 K.
[c]Reference 4, $T<295$ K.
[d]Present work, between 100 and 700 K.
[e]Present work, between 100 and 550 K.
[f]Present work; the larger value corresponds to a 2D mixture and the lower to a 2D maximum.
[g]P. Y. Yu and M. Cardona, Phys. Rev. B 2, 3193 (1970), calculated using only Debye-Waller terms.
[h]Reference 26, calculated using only Debye-Waller terms.

and Θ decrease. Experimental points at lower temperatures would be necessary to obtain this quadratic contribution for the E_2 structure. On the other hand, a more complicated formula than Eqs. (2) and (3) and that in Ref. 48 may be necessary to describe the temperature dependence in these materials.

The phase angle $\phi(E_2)$ is displayed in Fig. 10; ϕ runs nearly parallel to the angle for the E_1 CP (open circles). This angle, as chosen by us, represents, for $\pi/2<\phi<\pi$, the amount of 2D maximum added to a saddle point. Its temperature dependence may indicate that excitonic effects are also important at the E_2 CP. However, the complicated character of this CP prevents us from attributing this fact to a pure excitonic effect.

D. E_1' transitions

These transitions take place from the top valence band (Λ_3^v) to the second-lowest conduction band (Λ_3^c) near the L point. Unfortunately, our spectral region only covers the E_1' and $E_1'+\Delta_1'$ structures. We see two structures in Fig. 5: the largest [$E_1'=5.22(3)$ eV at 100 K] corresponds to transitions from $\Lambda_{4,5}^v$ to Λ_6^c, and the weakest [5.38(2) eV at 100 K] to transitions from $\Lambda_{4,5}^v$ to $\Lambda_{4,5}^c$. Its energy separation of 154(28) meV is somewhat lower than the calculated SO splitting [$\Delta_1'=240$—330 meV (Refs. 6 and 60)]. We have analyzed these transitions with a mixture of a 2D maximum and a saddle point. Within the experimental error the phase angle is found to be constant with a value of $\phi=47°\pm6°$. As we can see in Fig. 7 and Table I, the E_1' transition is more nonlinear at low temperatures than the other transitions observed for InSb, and its slope is also the largest. In Fig. 7 the solid line corresponds to a fit with Eq. (2a), the dashed line, with Eq. (2b). Again, measurements at liquid-He temperatures are needed in order to decide which of the two fits is better. The broadening parameter Γ and its temperature dependence are shown in the upper part of Fig. 9, as obtained with Eq. (3) (dashed line), where Θ has also been fixed to have the value obtained from the CP energy fit. The solid line in this figure corresponds to a linear fit.

In Table VI we list the average *linear* temperature coefficients of the CP energies in InSb in the (100—700)-K range, together with corresponding values found in the literature. Although there is a good agreement between our values and those given elsewhere for the E_1, $E_1+\Delta_1$, and E_2 critical points, our complete line-shape analysis should give better results than the maxima of observed peaks used so far in the literature. No previous data are available for the linear coefficients of the $E_0'(\Delta)$, $E_0'+\Delta_0'(\Delta)$, and E_1' critical points, and the corresponding broadening parameters.

IV. CONCLUSIONS

We have analyzed, by means of spectral ellipsometry, the temperature dependence of the dielectric function of InSb. Detailed information about this dependence and accurate values of the complex dielectric function between 100 and 700 K have been presented. The different contributions of Γ and Δ symmetry in the E_0' region have been obtained. The critical-point energies and broadening parameters of the E_1, $E_1+\Delta_1$, E_0', $E_0'+\Delta_0'$, E_2, and E_1' transitions have been analyzed by studying the line shape of the second-derivative spectra. With increasing temperature, a rapid decrease of excitonic effects for the E_1, E_0', and E_2 structures is found, with a smaller decrease for the $E_1+\Delta_1$. These effects are found to be independent of temperature for the E_1' structure.

ACKNOWLEDGMENTS

We would like to thank H. Höchst and W. Neu for help with the construction of the cryostat, G. Kisela and coworkers at the Max-Planck-Institute for sample preparation, and M. Bleder and A. Birkner for help with the construction of the ellipsometer. We would also like to thank H. Hirt, M. Siemers, and P. Wurster for expert technical help.

*On leave from First Laboratory of Physics, Aristotle University of Thessaloniki, Thessaloniki, Greece.

[1]T. S. Moss and T. D. H. Hawkins, Proc. Phys. Soc. London **72**, 270 (1957).

[2]F. Lukeš and E. Schmidt, in *Proceedings of the 6th International Conference on the Physics of Semiconductors, Exeter, 1962,* edited by A. C. Stickland (The Institute of Physics and the Physical Society, London, 1962), p. 389.

[3]D. L. Greenaway and M. Cardona, in *Proceedings of the 6th International Conference on the Physics of Semiconductors, Exeter, 1962,* Ref. 2, p. 666.

[4]M. Cardona and G. Harbeke, J. Appl. Phys. **34**, 813 (1963).

[5]J. Camassel and D. Auvergne, Phys. Rev. B **12**, 3258 (1975); D. Auvergne, J. Camassel, H. Mathieu, and M. Cardona, *ibid.* **9**, 5168 (1974).

[6]M. Cardona, K. L. Shaklee, and F. H. Pollak, Phys. Rev. **154**, 696 (1967).

[7]E. Matatagui, A. G. Thompson, and M. Cardona, Phys. Rev. **176**, 950 (1968).

[8]G. Guizetti, L. Nosenzo, E. Regguzoni, and G. Samoggia, Phys. Rev. B **9**, 640 (1974).

[9]C. R. Pidgeon, S. H. Groves, and J. Feinleib, Solid State Commun. **5**, 677 (1967).

[10]K. L. Shaklee, J. E. Rowe, and M. Cardona, Phys. Rev. **174**, 828 (1968).

[11]R. R. L. Zucca and Y. R. Shen, Phys. Rev. B **1**, 2668 (1970).

[12]M. Welkowsky and R. Braunstein, Phys. Rev. B **5**, 497 (1972).

[13]H. J. Mattausch and D. E. Aspnes, Phys. Rev. B **23**, 1896 (1981).

[14]V. M. Bermúdez and V. H. Ritz, Phys. Rev. B **26**, 3297 (1982).

[15]S. Zimmermann, J. Phys. C **9**, 2643 (1976).

[16]H. Höchst and I. Hernández-Calderón, Surf. Sci. **126**, 25 (1983).

[17]J. C. Phillips, Phys. Rev. **125**, 1931 (1962).

[18]M. L. Cohen and T. K. Bergstresser, Phys. Rev. **141**, 789 (1966).

[19]C. W. Higginbotham, F. H. Pollak, and M. Cardona, in *Proceedings of the 9th International Conference on the Physics of Semiconductors, Moscow, 1968* (Publishing House of the

Academy of Sciences of the USSR, Leningrad, 1968), p. 57.
[20]J. R. Chelikowsky and M. L. Cohen, Phys. Rev. B **14**, 556 (1976); J. Chelikowsky, D. J. Chadi, and M. L. Cohen, *ibid.* **8**, 2786 (1973).
[21]M. L. Cohen and D. J. Chadi, in *Semiconductor Handbook,* edited by M. Balkanski (North-Holland, Amsterdam, 1980), Vol. 2, Chap. 4B.
[22]P. B. Allen and V. Heine, J. Phys. C **9**, 2305 (1976).
[23]P. B. Allen and M. Cardona, Phys. Rev. B **27**, 4760 (1983).
[24]H. Y. Fan, Phys. Rev. **82**, 900 (1951).
[25]J. P. Walter, R. R. L. Zucca, M. L. Cohen, and Y. R. Shen, Phys. Rev. Lett. **24**, 102 (1970).
[26]Y. F. Tsay, B. Gong, S. S. Mitra, and J. F. Vetelino, Phys. Rev. B **6**, 2330 (1972).
[27]K. Baumann, Phys. Status Solidi B **63**, K71 (1974).
[28]D. E. Aspnes, Opt. Commun. **8**, 222 (1973); D. E. Aspnes and A. A. Studna, Appl. Opt. **14**, 220 (1975).
[29]L. Viña, S. Logothetidis, and M. Cardona, Phys. Rev. B **30**, 1979 (1984).
[30]D. E. Aspnes and A. A. Studna, Phys. Rev. B **27**, 985 (1983).
[31]D. E. Aspnes, J. Vac. Sci. Technol. **17**, 1057 (1980).
[32]D. E. Aspnes and A. A. Studna, Appl. Phys. Lett. **39**, 316 (1981).
[33]H. G. Gatos and M. C. Lavine, Surf. Char. Comp. **107**, 433 (1960); **107**, 427 (1960).
[34]C. W. Wilmsen, J. Vac. Sci. Technol. **19**, 279 (1981).
[35]N. M. Bashara and R. M. Azzam, in *Ellipsometry and Polarized Light* (North-Holland, Amsterdam, 1977).
[36]Leitsilber 200, Demetron, Leipzigerstrasse 10, D-6450 Hanau, Federal Republic of Germany.
[37]M. Cardona and H. S. Sommers, Jr., Phys. Rev. **122**, 1382 (1961).
[38]Y. Toyozawa, M. Inoue, T. Inui, M. Okazaki, and E. Hanamura, J. Phys. Soc. Jpn. **22**, 1337 (1967).
[39]M. Cardona, in *Modulation Spectroscopy,* Supplement 11 of *Solid State Physics,* edited by F. Seitz, D. Turnbull, and H. Ehrenreich (Academic, New York, 1969).
[40]L. Viña, H. Höchst, and M. Cardona, following paper, Phys. Rev. B **31**, 958 (1985).
[41]D. E. Aspnes, in *Semiconductor Handbook,* Ref. 21, Vol. 2, Chap. 4A.
[42]Y. P. Varshni, Physica (Utrecht) **34**, 149 (1967).
[43]H. Ehrenreich, H. R. Philipp, and J. C. Phillips, Phys. Rev. Lett. **8**, 59 (1962).
[44]S. O. Sari and S. E. Schnatterly, Surf. Sci. **37**, 328 (1973).
[45]D. E. Aspnes and A. A. Studna, Phys. Rev. B **7**, 4605 (1973).
[46]D. E. Aspnes, C. G. Olson, and D. W. Lynch, Phys. Rev. B **14**, 4450 (1976).
[47]U. Piesberger, in *Semiconductors and Semimetals,* edited by R. K. Willardson and A. C. Beer (Academic, New York, 1966), Vol. 2, Chap. 3.
[48]A. Manoogian and A. Leclerc, Can J. Phys. **57**, 1766 (1979); Phys. Status Solidi B **92**, K23 (1979).
[49]D. L. Price, J. M. Rowe, and R. M. Nicklow, Phys. Rev. B **3**, 1268 (1971); K. Kunc, M. Balkanski, and M. A. Nusimovici, Phys. Status Solidi B **72**, 229 (1975).
[50]E. O. Kane, Phys. Rev. **180**, 852 (1969).
[51]S. M. Kelso, D. E. Aspnes, M. A. Pollak, and R. E. Nahory, Phys. Rev. B **26**, 6669 (1982).
[52]J. E. Rowe and D. E. Aspnes, Phys. Rev. Lett. **25**, 162 (1970).
[53]M. Cardona, in *Light Scattering in Solids II,* edited by M. Cardona and G. Güntherodt (Springer, New York, 1982), p. 119.
[54]M. Cardona, Phys. Rev. B **15**, 5999 (1977).
[55]A. Daunois and D. E. Aspnes, Phys. Rev. B **18**, 1824 (1978).
[56]D. E. Aspnes and M. Cardona, Solid State Commun. **27**, 397 (1978).
[57]W. Hanke and L. J. Sham, Phys. Rev. B **21**, 4656 (1980).
[58]D. E. Aspnes, Phys. Rev. B **12**, 2297 (1975).
[59]*Landolt-Börnstein* (new series), edited by O. Madelung (Springer, Berlin, 1982), Vol. 17a.
[60]G. G. Wepfer, T. C. Collins, and R. N. Euwema, Phys. Rev. B **4**, 1296 (1971).